A new predictive equation for estimating wave period of subaerial solid-block landslide-generated waves

Ramtin Sabeti*[1], Mohammad Heidarzadeh[2]

[1] Department of Civil and Environmental Engineering, Brunel University London, UB8 3PH Uxbridge, UK
[2] Department of Architecture and Civil Engineering, University of Bath, Bath BA2 7AY, UK

Published in: "**Coastal Engineering Journal**"

https://doi.org/10.1080/21664250.2022.2110657

***Corresponding author:**

Ramtin Sabeti
Department of Civil and Environmental Engineering,
Brunel University London,
Howell Building, Room 308,
UB8 3PH Uxbridge,
United Kingdom.
Email: ramtin.sabeti@brunel.ac.uk
Tel: +44-7498011445
ORCID: https://orcid.org/0000-0002-8154-7512

Abstract

In the aftermath of the deadly 2018 Anak Krakatau tsunami (Indonesia) and associated confusions over its modelling and generation mechanism, there has been an urgent need for further studies to improve our understanding of landslide-generated tsunamis. Two important factors in accurate modelling of landslide tsunamis are the wave period and the initial wave amplitude. Here, we apply a physical modelling approach and develop an empirical equation to predict the dominant wave period generated by solid-block subaerial landslide tsunamis. Fifty-one laboratory experiments are conducted at different water depths and using four different concrete blocks for the sliding masses. The results are consequently employed to derive a predictive equation for the wave period of solid-block subaerial landslide tsunamis. An innovation of this study is that we apply data from different scales (laboratory and field scales) to produce our predictive equation. For field data, the data from the 2018 Anak Krakatau event is used. We compared our predictive equation with other previously-published equations. To confirm the validity of our predictive equation, it is applied for the prediction of the wave period of an independent landslide tsunami event whose data was not used for the derivation of the equation.

Keywords: Tsunami; Landslide; Volcano; Physical modelling.

1-Introduction and literature review

The recent 2018 Anak Krakatau and Palu landslide tsunamis highlighted potential large tsunami hazards from subaerial and submarine landslides (Takagi et al., 2019; Muhari et al., 2019; Grilli et al., 2021; Zengaffinen et al., 2020; Mulia et al., 2020; Aránguiz et al., 2020). These so-called atypical tsunamis, which are generated by non-seismic sources such as volcanos and landslides, have been responsible for thousands of fatalities since 1998 with major deadly tsunamis such as the 1998 Papua New Guinea (over 2,000 deaths) (Synolakis et al., 2002; Heidarzadeh and Satake, 2015), the September 2018 Palu (over 4,000 deaths) (Aránguiz et al., 2020) and the December 2018 Anak Krakatau (more than 430 deaths) (Grilli et al., 2021). A major challenge with tsunamis from non-seismic sources is that their generation mechanism is not well understood and thus the predictive tools are not adequately developed. For example, this challenge has been witnessed following the 2018 Anak Krakatau event where a wide range of source wave amplitudes (from 10 m to over 100 m) have been proposed by different authors (Grilli et al., 2019, 2021; Ren et al., 2020; Heidarzadeh et al., 2020; Paris et al., 2020). It has been the motivation of this study to further work on understanding the generation mechanism of tsunamis from subaerial landslides.

Many existing studies have focused on physical experiments to present a relationship between impulse wave amplitudes (a_M) and landslide parameters (Figure 1). A wide variety of experimental conditions has been considered in these investigations including two- and three-dimensional physical tests that assume the landslide as solid blocks (e.g. Noda, 1970; Panizzo et al., 2005; Saelevik et al., 2009; Heller and Spinneken, 2015) or granular materials (e.g. Fritz et al., 2004; Mohammed and Fritz, 2012; McFall and Fritz, 2016; Takabatake et al., 2020). A number of empirical equations were derived using such datasets for the prediction of maximum wave amplitudes generated by subaerial landslides (Fritz et al., 2004; Heller and Hager, 2011; Mulligan and Take, 2017; Bullard et al., 2019). Conversely, there are only a few researches that focused on the prediction of wave period although both wave amplitudes and wave periods (wavelengths) are essential for modelling landslide-generated waves. For example, an important parameter for modelling landslide tsunamis is the dimension of the initial source, which is usually calculated by knowing the wave period (e.g., Heidarzadeh et al., 2020). Therefore, knowledge of wave period is essential for modelling landslide tsunamis. Among researchers who studied wave periods of solid-block landslide-generated waves are Ataie-Ashtiani and Nik-Khah (2008) and Heller and Spinneken (2013 and 2015).

As limited information is available on this topic, this study is focused on the understanding of the relationships between landslide parameters and wave period for solid-block subaerial landslide-generated waves. Inspired by the 2018 Anak Krakatau event, which is widely considered as a subaerial solid-block landslide tsunami, this research is devoted to subaerial solid-block landslide tsunamis. We conducted an intensive physical experimental study and delivered 51 tests, analysing them towards developing a predictive equation. We considered the two most important landslide parameters in this study for developing our predictive equation comprising landslide volume (V) and landslide Froude number (F). We note that our equation also includes water depth (h) as we nondimensionalized the landslide volume using water depth. Scale effects on the experiments were studied. We compared our predictive equation with those previously published in the literature.

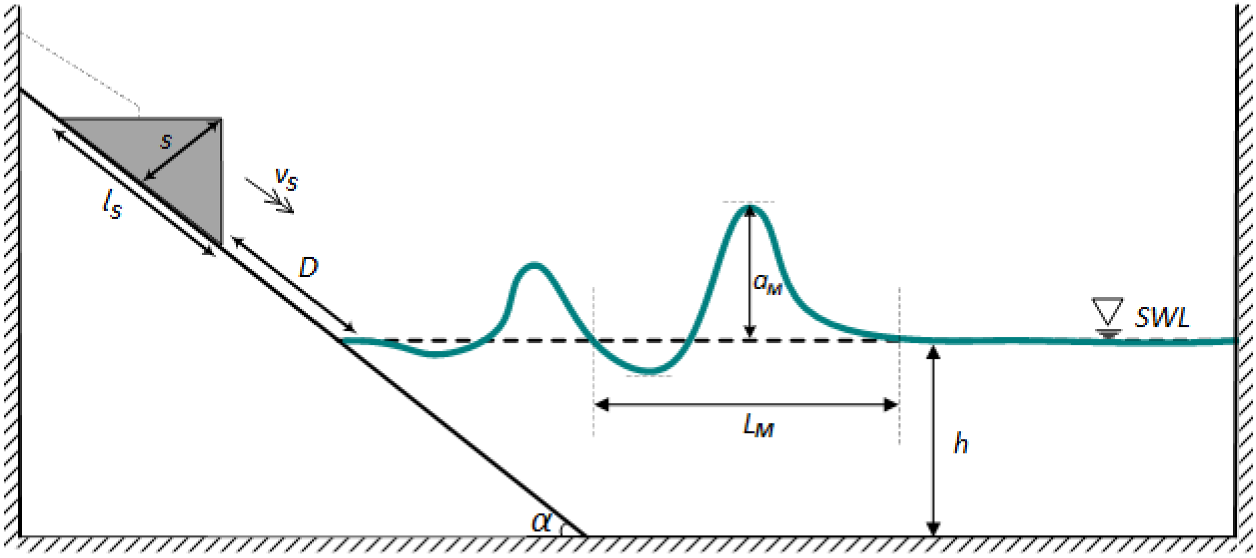

Figure 1. Sketch showing the geometrical and kinematic parameters of a subaerial landslide tsunami. Parameters are: h, water depth; a_M, maximum wave amplitude; α, slope angle; L_M, dominant wavelength; l_s, length of slide; D, travel distance (the distance from toe of the sliding mass to the water surface); and SWL, still water level.

2- Data and Methods

This research is based on physical modelling of subaerial solid-block landslide-generated waves in a wave flume at Brunel University London (UK) (Figure 2). We conducted 51 tests of subaerial landslides by changing the volume of the sliding mass (Table 1), the water depth and the Froude number and recorded wave time series. In order to increase the reliability of the experiments we repeated each test for three times. The wave flume is 0.26 m wide, 0.50 m deep and 6.0 m long (Figure 2). The sliding masses are made from concrete with a density of 2,600 kg/m^3 and at four different sizes (Table 1; Figure 2b). The slope angle of the incline was fixed at 30^o in our study. This slope angle was selected assuming that it is an average slope angle for most subaerial landslide incidents. By changing the water depth in the range of 0.06 m – 0.31 m, applying four sliding masses ($V1$- the smallest, $V2$, $V3$ and $V4$- the largest) and changing the velocity of the sliding masses, we tested 51 scenarios for our physical modelling (Table 2). Twenty-five of the tests were performed by releasing the blocks from the rest position at the top of the slope and allowing free movement under gravity. The rest of the tests were conducted by controlling the velocity of the masses. To change the velocity of slides, a rope was connected to a hook on the top of the solid blocks in order to control the movement of the slide and to generate different Froud numbers for various experiments. The rationale for conducting the controlled tests was to change the velocity of the mass (v_s) for each test and consequently to provide a range for the Froude number (F), which is defined as:

$$F = \frac{v_s}{\sqrt{gh}} \quad (1)$$

where F is Froude number, v_s is the velocity of the sliding mass which varies for each test, g is the gravitational acceleration, and h is water depth. The time interval for each test is the period of time starting from the release time of the mass until the toe of the mass touches the bottom of the flume; this time interval was used to calculate the average velocity for each test. We used the videos of the experiments, recorded by a camera (model Sony A6300) with a sampling frequency of 120 frames per second, to measure the average velocity of the sliding blocks. The wave times series were recorded at a wave gauge of the model HRIA-1016 from HR Wallingford Inc. (http://equipit.hrwallingford.com/products/wave-gauges), located at the distance of 0.40 m from the toe of the incline (Figure 2a).

As the water waves generated by landslides may involve a few signals with different wave periods, we focus on reporting the dominant wave period in this study, which essentially means the longest period in the wave spectrum. To calculate the dominant wave period of the recorded landslide-generated waves, we employed the Fast Fourier Transform (FFT) algorithm of the MATLAB package (the command 'fft' in MathWorks, 2022). As the wave flume was 6.0 m long, the later phases of the recorded waveforms were the reflected waves; therefore, we used only the first few waves before the arrival of the reflected waves. For fitting curves to the experimental data points, we applied the Nonlinear least-square regression model among the 'fit-options' collection in the MATLAB package (MathWorks, 2022) to establish relationships between wave period and individual landslide parameters. The powers of the relationships for individual parameters were applied for developing our final predictive equation. To develop the final predictive equation, which is a multi-variant equation, we used the stochastic optimization technique of Genetic Algorithm embedded in MathWorks (2022).

Figures 3 and 4 demonstrate the time series for all of the physical experiments by classifying the waveforms into two categories studying the impacts of landslide volume (Figure 3), and Froude number (Figure 4). Initial visual inspections of Figure 3 reveal that by increasing the volume of the sliding blocks, the wave amplitudes and wave periods increase. Regarding the effect of Froude number on the wave characteristic, visual inspections of Figure 4 reveal that wave period increases by a decrease in Froude number; wave amplitude increases by an increase in Froude number. We performed FFT analyses to quantify the dominant wave periods which are presented in the next Section. A 3D representation of the experiments is shown in Figure 5 mapping the maximum wave amplitudes (a_M) relative to volumes of the landslide blocks (V) and water depth (h). As it is long known, landslide-generated waves show nonlinear behaviour (Frtiz et al., 2004). We studied the nonlinearity of the waves in our experiments by calculating the Ursell number ($U = a_M \, {L_M}^2/h^3$), where $L_M = \frac{g\,T_M^2}{2\,\pi}\tanh(\frac{2\,\pi}{L_M}h)$ is dominant wavelength, h is water depth, and a_M is maximum wave amplitude (Table 3). Normally Ursell number is less than one for linear waves (Fritz et al., 2004). For nonlinear waves, a larger Ursell number is expected ($U > 1$). Table 3 reveals that 94% of our experiments result in $U > 1$, indicating that they show nonlinear behaviour.

It is known that experimental studies are subject to scale effects, which could cause deviations of the laboratory results from the real world (Hughes, 1993; Heller, 2011). Therefore, it is important to study potential scale effects and ensure that they are within acceptable ranges. According to Hughes (1993) and Heller (2011), most of the Coastal Engineering problems can be readily experimented in a hydraulic laboratory applying Froude similitude. However, in some cases, the scale effects can be significant; for instance, in modelling waterfalls and spillways, which normally experience significant air entrainments. For our physical experiments, we studied scale effects by comparing the results in different scales (Figure 6). For this analysis, we selected pairs of experiments with similar nondimensional parameters M_s (nondimensional mass, $M_s = m_s/(\rho_w w h^2)$, where m_s is the slide mass, w is slide width), F (Froude number based on Equation 1) and S (nondimensional slide thickness, $S = s/h$, where s is slide thickness, Figure 1) according to the method practiced by Heller and Hager (2011). The waveforms are nondimensionalised for this analysis (Figure 6). A pair of experiments at a scale ratio of 0.57 (Figure 6a), and another pair at a scale ratio of 0.56 (Figure 6b) are studied. According to Figure 6, the scale effects appeared to be negligible for both cases.

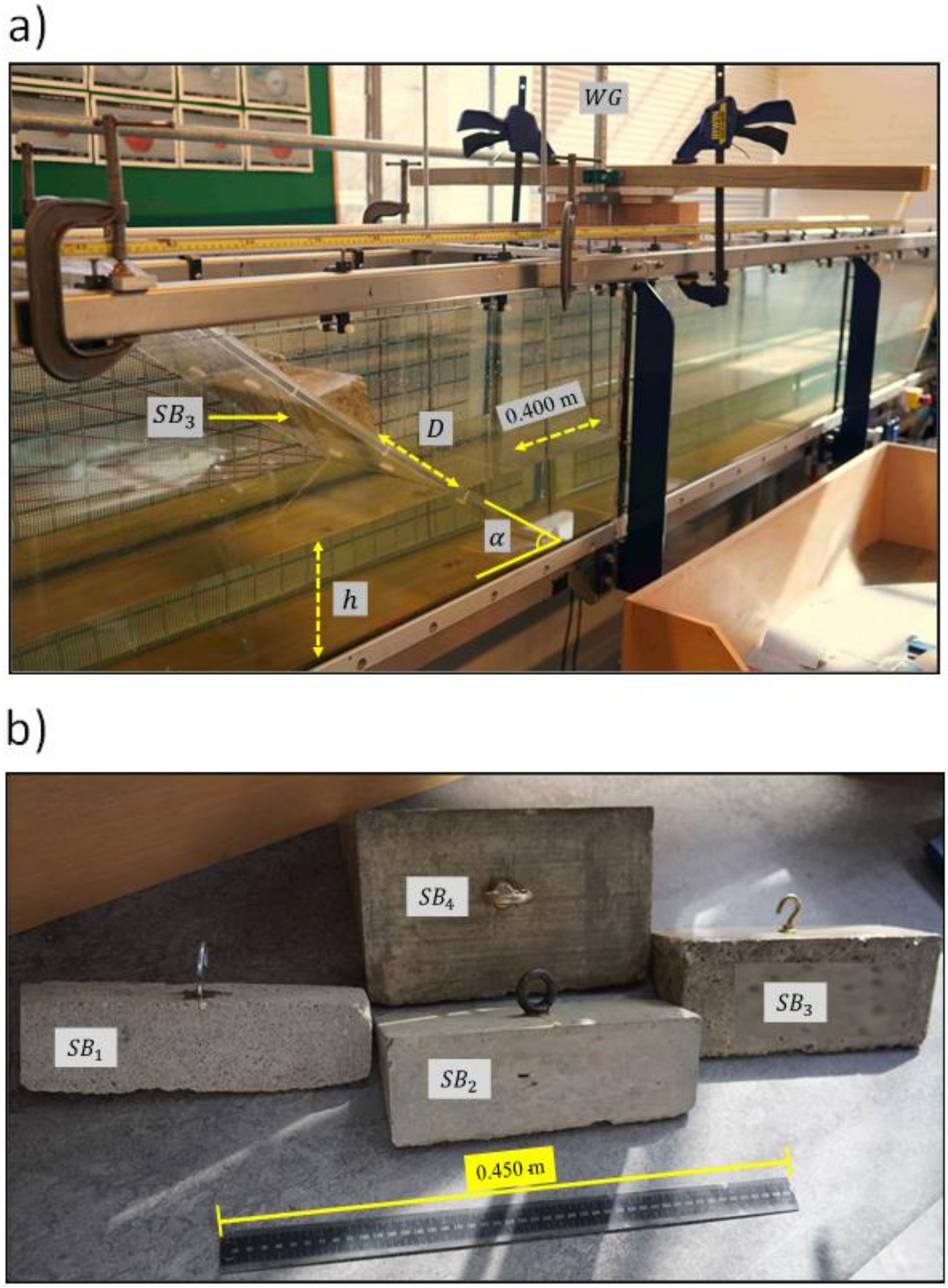

Figure 2. Wave flume used in this study for physical experiments showing the wave gauge (WG), the slope **(a),** and the four sliding blocks **(b)**. Parameters are: h, water depth; D, travel distance (the distance from toe of the sliding mass to the water surface); SB_{1-4}, Solid blocks (see Table 1 for their dimensions). The distance between the toe of slope and the wave gauge is 0.40 m.

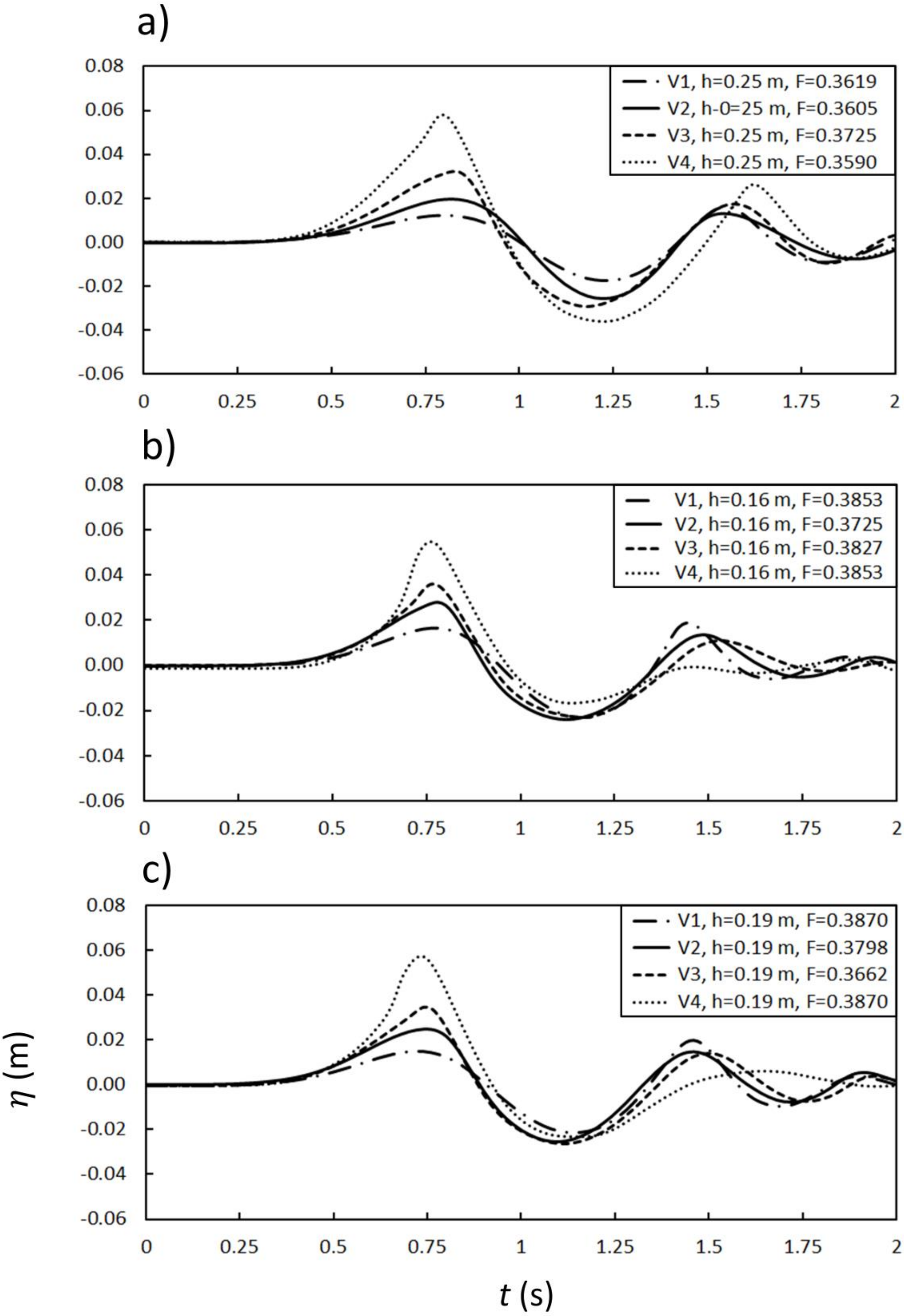

Figure 3. Studying the effect of landslide volume on the experimental water waveforms recorded for the solid-block subaerial landslide-generated waves during the physical modelling using different concrete blocks with volumes V_1 - V_4 (Table 1) at different water depths (h) and Froude numbers (F). The horizontal axis shows time (t), and the vertical axis shows wave amplitude (η).

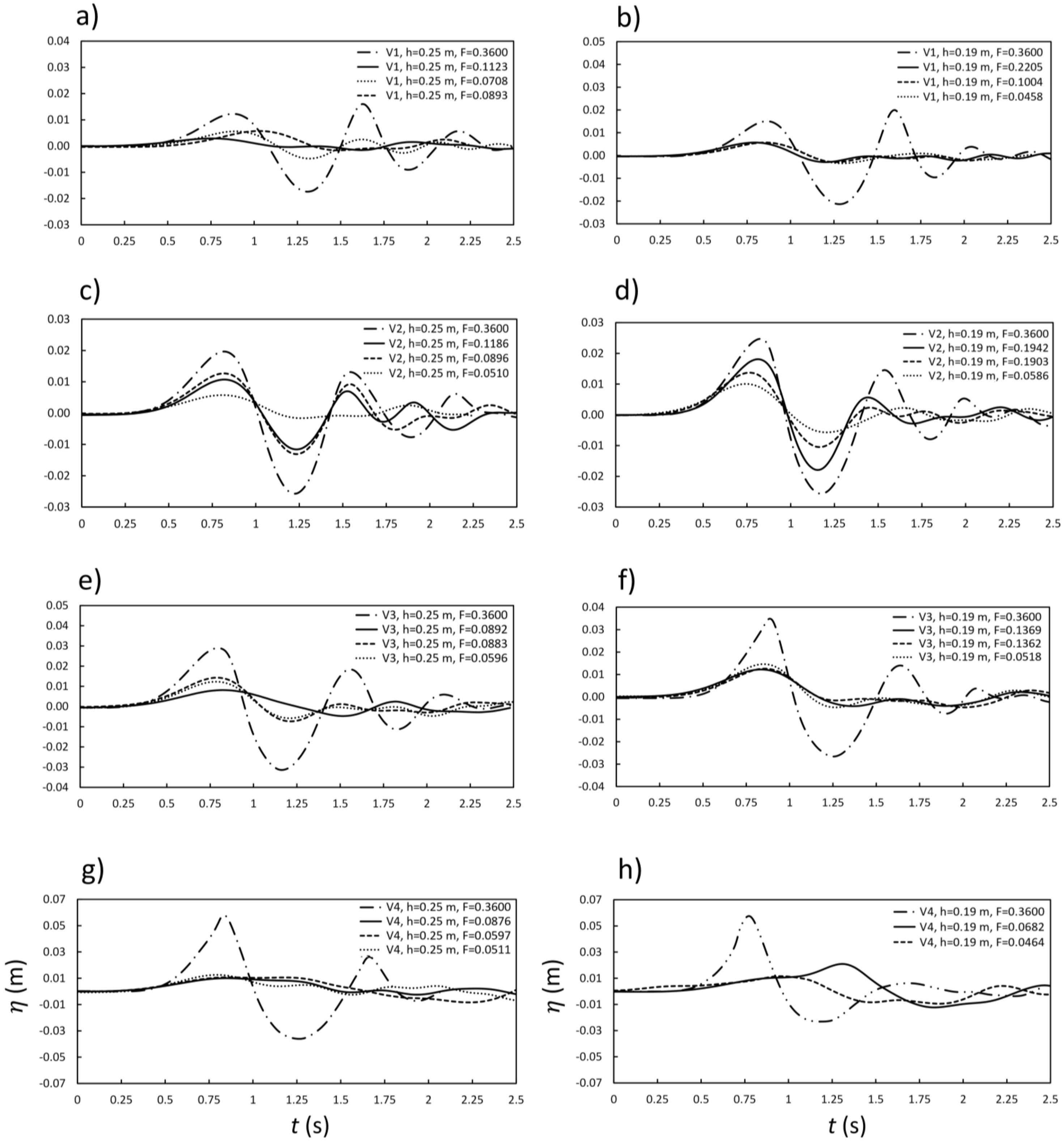

Figure 4. Studying the effect of Froude number on the experimental water waveforms recorded for solid-block subaerial landslide-generated waves during the physical modelling using different concrete blocks with volumes V_1 - V_4 (Table 1), different water depths (h) and Froude numbers (F). The horizontal axis shows time (t), and the vertical axis shows wave amplitude (η).

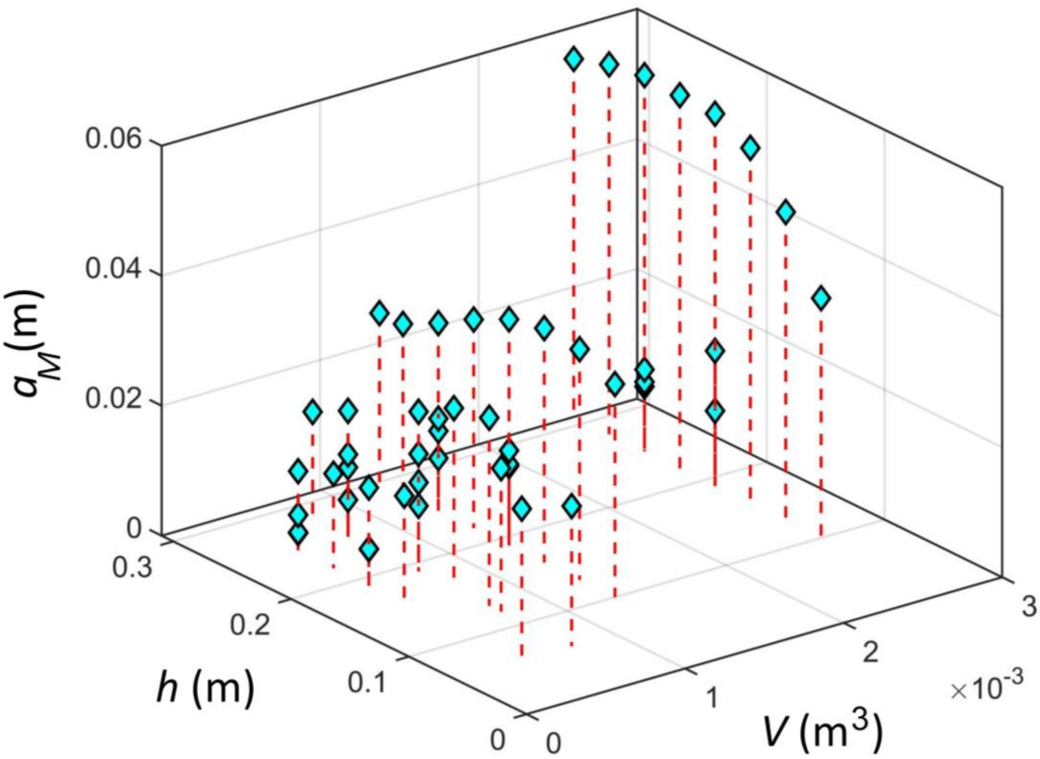

Figure 5. A 3D projection of the maximum wave amplitudes (a_M) of our experimental data versus solid block volumes (V) and water depths (h).

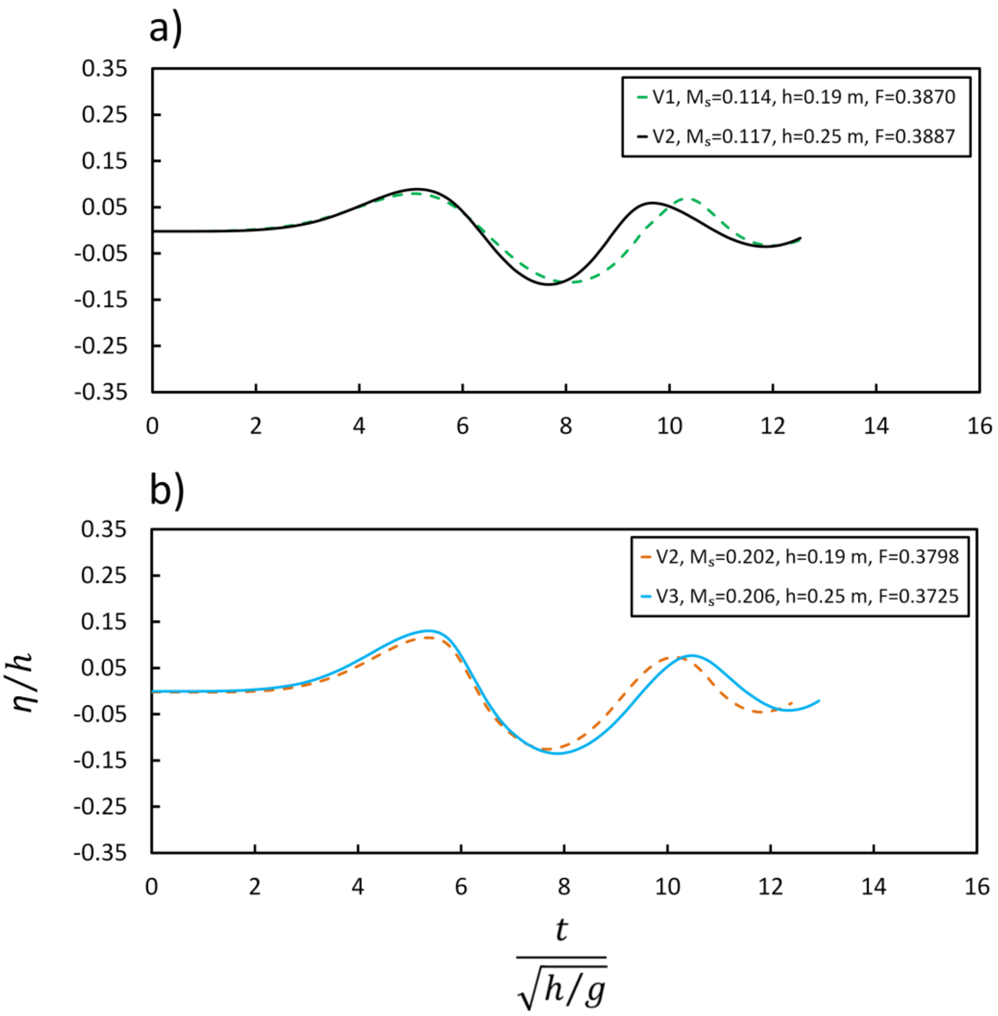

Figure 6. Nondimensional waveforms for pairs of physical experiments with similar nondimensional mass (M_s) and Froude number (F) as a way to study scale effects during our physical modelling. V_1, V_2 and V_3 are different concrete blocks (Table 1), h is water depth, η is wave amplitude, t is time, and g is gravitational acceleration.

Table 1. Geometrical information of the four solid blocks used for landslide physical experiments in this study.

Solid block*	l_s (m)	w (m)	s (m)	V (m^3)	γ_s	m_s (kg)
Block-1	0.080	0.26	0.040	4.16×10^{-4}	2.60	1.065
Block-2	0.106	0.26	0.053	7.30×10^{-4}	2.60	1.895
Block-3	0.141	0.26	0.071	1.30×10^{-3}	2.60	3.350
Block-4	0.200	0.26	0.100	2.60×10^{-3}	2.60	6.760

***:** Parameters are: l_s, slide length; w, slide width; s, slide thickness; V, slide volume, $\gamma_s = \rho_s/\rho_w$, slide specific gravity, ρ_w=1000 kg/m^3, density of water, ρ_s=2600 kg/m^3, density of slide, and m_s is slide mass.

Table 2. The experimental program for the 51 physical tests performed in this study for subaerial solid-block landslide-generated waves. All experiments are conducted using a slope angle of 30°. Parameters are: F, Froude number; h, water depth; D, travel distance (the distance from toe of the sliding mass to the water surface); T_M, dominant wave period; a_M, maximum wave amplitude; $M_s = m_s/\rho_w wh^2$, nondimensional mass; m_s, slide mass; ρ_w =1000 kg/m^3, density of water; w, slide width; h, water depth; L_M, dominant wavelength; and U, Ursell number. See Figure 1 for the sketch showing some of these parameters.

Test No	Block No	F	h (m)	D (m)	T_M (s)	a_M (m)	M_s	L_M (m)	U	Mechanism
1	Block-1	0.3619	0.25	0.14	0.50	0.0123	0.066	0.69	0.37	Gravity
2	Block-1	0.0708	0.25	0.14	1.11	0.0078	0.066	1.5	1.12	Controlled
3	Block-1	0.1123	0.25	0.14	0.74	0.0029	0.066	0.86	0.14	Controlled
4	Block-1	0.0893	0.25	0.14	0.73	0.0076	0.066	0.8	0.31	Controlled
5	Block-1	0.3827	0.22	0.14	0.67	0.0146	0.085	0.89	1.09	Gravity
6	Block-1	0.3870	0.19	0.14	0.50	0.0151	0.114	0.69	1.05	Gravity
7	Block-1	0.0458	0.19	0.14	1.14	0.0056	0.114	1.40	1.60	Controlled
8	Block-1	0.1004	0.19	0.14	1.08	0.0056	0.114	1.31	1.40	Controlled
9	Block-1	0.2205	0.19	0.14	1.06	0.0057	0.114	1.28	1.36	Controlled
10	Block-1	0.3853	0.16	0.14	0.58	0.0165	0.160	0.51	1.05	Gravity
11	Block-1	0.3724	0.06	0.14	0.52	0.0234	1.139	0.34	12.52	Controlled
12	Block-2	0.3650	0.06	0.14	0.50	0.0216	2.028	0.32	10.24	Controlled
13	Block-2	0.3641	0.28	0.14	0.53	0.0166	0.093	0.74	1.41	Gravity
14	Block-2	0.3887	0.25	0.14	0.67	0.0214	0.117	0.90	1.11	Gravity
15	Block-2	0.0510	0.25	0.14	0.89	0.0237	0.117	1.10	1.84	Controlled
16	Block-2	0.0896	0.25	0.14	0.65	0.0227	0.117	0.89	1.15	Controlled
17	Block-2	0.1186	0.25	0.14	0.61	0.0407	0.117	0.70	1.28	Controlled
18	Block-2	0.3795	0.12	0.14	0.65	0.0221	0.507	0.57	4.16	Controlled
19	Block-2	0.3798	0.19	0.14	0.63	0.0246	0.202	0.60	1.29	Gravity
20	Block-2	0.0586	0.19	0.14	0.77	0.0101	0.202	0.83	1.01	Controlled
21	Block-2	0.1903	0.19	0.14	0.69	0.0137	0.202	0.80	1.28	Controlled
22	Block-2	0.1942	0.19	0.14	0.61	0.0181	0.202	0.90	2.14	Controlled
23	Block-2	0.3725	0.16	0.14	0.61	0.0278	0.285	0.55	2.05	Gravity
24	Block-2	0.3646	0.13	0.14	0.65	0.029	0.432	0.58	4.44	Gravity
25	Block-3	0.3886	0.30	0.14	0.69	0.046	0.143	0.85	1.23	Gravity
26	Block-3	0.3840	0.28	0.14	0.71	0.0381	0.165	0.77	1.03	Gravity
27	Block-3	0.3725	0.25	0.14	0.67	0.0289	0.206	0.79	1.15	Gravity
28	Block-3	0.0892	0.25	0.14	1.25	0.0081	0.206	1.75	1.59	Controlled
29	Block-3	0.0596	0.25	0.14	1.13	0.0123	0.206	1.54	1.87	Controlled
30	Block-3	0.0883	0.25	0.14	1.08	0.0142	0.206	1.45	1.91	Controlled
31	Block-3	0.3767	0.22	0.14	0.64	0.0321	0.267	0.62	1.16	Gravity
32	Block-3	0.3662	0.19	0.14	0.62	0.0348	0.357	0.58	1.71	Gravity
33	Block-3	0.1362	0.19	0.14	1.41	0.0125	0.357	1.80	5.90	Controlled
34	Block-3	0.1369	0.19	0.14	1.06	0.0122	0.357	1.28	2.91	Controlled
35	Block-3	0.0518	0.19	0.14	1.08	0.0146	0.357	1.31	3.65	Controlled
36	Block-3	0.3827	0.16	0.14	0.64	0.0361	0.504	0.60	3.17	Gravity
37	Block-3	0.3874	0.13	0.14	0.71	0.0355	0.763	0.66	7.04	Gravity
38	Block-3	0.3624	0.10	0.14	0.51	0.0328	1.290	0.38	4.74	Gravity
39	Block-4	0.3649	0.31	0.14	0.71	0.0551	0.271	0.78	1.13	Gravity
40	Block-4	0.3610	0.28	0.14	0.71	0.0569	0.332	0.77	1.54	Gravity
41	Block-4	0.3590	0.25	0.14	0.71	0.0579	0.416	0.76	2.14	Gravity
42	Block-4	0.0511	0.25	0.14	1.51	0.0107	0.416	2.19	3.28	Controlled
43	Block-4	0.0597	0.25	0.14	1.47	0.01	0.416	2.12	2.88	Controlled
44	Block-4	0.0876	0.25	0.14	1.41	0.0126	0.416	2.02	3.29	Controlled

45	Block-4	0.3827	0.22	0.14	0.68	0.0575	0.537	0.69	2.57	Gravity
46	Block-4	0.3870	0.19	0.14	0.82	0.0573	0.720	0.91	6.92	Gravity
47	Block-4	0.0464	0.19	0.14	1.28	0.0116	0.720	1.61	4.38	Controlled
48	Block-4	0.0682	0.19	0.14	1.41	0.0208	0.720	1.80	9.83	Controlled
49	Block-4	0.3853	0.16	0.14	0.58	0.0547	1.016	0.51	3.47	Gravity
50	Block-4	0.3874	0.13	0.14	0.80	0.0475	1.538	0.78	13.15	Gravity
51	Block-4	0.3820	0.10	0.14	0.52	0.0369	2.600	0.39	5.61	Gravity

3- Results

The dominant wave periods for experimental waveforms are calculated using the FFT procedure whose results are given in Figure 7 and Table 2. The wave period is ranging from 0.50 s to 1.51 s for the 51 experiments (Table 2). The minimum wave period of 0.51 s belongs to the experiment with Block-1 (the smallest one) at the water depth of 0.25 m and under free gravity movement. The longest period of 1.51 s is achieved using Block-4 (the largest one) at the water depth of 0.25 m and under a controlled movement. The data in Table 2 reveals that the maximum wave period is three times longer than the minimum period, indicating that the experimental data are sufficiently separated from each other.

In order to study the relationship between wave period and the two landslide parameters of volume (V) and Froude number (F), we produced two plots from the experimental data as shown in Figure 7. The data resulted in a direct relationship between wave period and landslide volume with a relationship given in the following:

$$T_M/\sqrt{\frac{h}{g}} = 6.10\ (\frac{V}{h^3})^{0.678} \qquad (2)$$

where T_M is dominant wave period in seconds, V is landslide volume in m^3, g is gravitational acceleration (9.81 m/s^2), and h is water depth in m. Such a direct relationship between T_M and V was previously reported by Heller and Spinneken (2013). Simply, Equation (2) indicates that the larger the volume of a landslide, the longer the period of the generated wave will be.

Regarding the Froude number of the landslides (F), our experiments resulted in an inverse relationship between F and wave period as follows:

$$T_M/\sqrt{\frac{h}{g}} = 2.85\ F^{-0.492} \qquad (3)$$

where T_M is dominant wave period in seconds, g is gravitational acceleration (9.81 m/s^2), h is water depth in m, and F is the Froude number of the landslide calculated using Equation (1). We note that Heller and Spinneken (2013) reported a direct relationship between T_M and F whereas we found an inverse relationship between them. From the viewpoint of the physics of water waves, it appears that slower landslides, with lower Froude numbers, generate waves with longer periods. This has been confirmed through experimental studies of Van Nieuwkoop (2007).

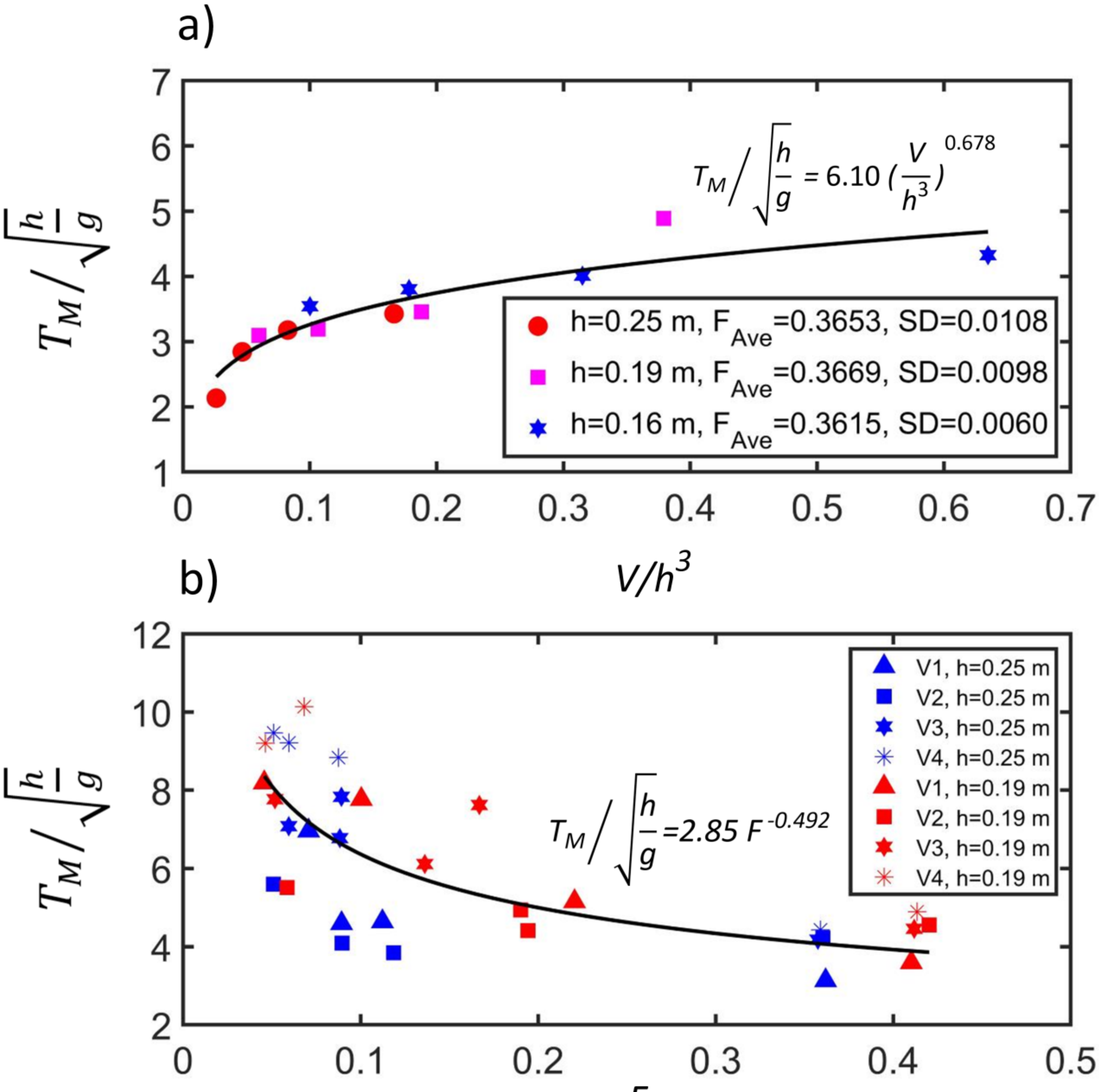

Figure 7. Curve fitting on the experimental data of dominant wave period (T_M). (**a**) The effect of volume of sliding mass (V) on the wave period. F_{Ave} is the average Froude number for each group of the tests. For this analysis, tests with the same release mechanism (i.e., gravity; $F \cong 0.36$) and the same water depth but with different slide volumes were grouped together. (**b**) The effect of Fronde number of the landslides (F) on the wave period. Here, h is water depth, and g is gravitational acceleration. For this analysis, tests with the same water depths and the same volumes but different Froude number were grouped together. SD is abbreviation for standard deviation.

4-The new predictive equation and discussions:

An innovation of this study is that we apply data from different scales (laboratory and field scales) to produce our predictive equation for the wave period of subaerial solid-block landslide-generated waves. Calibration and validation of empirical equations using field data is essential for ensuring that the equations can be successfully applied to real events. A challenge for these types of research has been lack of field data. However, there have been some subaerial landslide tsunamis in the past few years such as the December 2018 Anak Krakatau tsunami which provided actual field data. Several authors provided field data and numerical simulations for the 2018 Anak Krakatau event (Grilli et al. 2019, 2021; Heidarzadeh et al. 2020; Mulia et al. 2020; Paris et al. 2020). The wave period of this tsunami is calculated as in the range of 6.3 – 8.9 min by Heidarzadeh et al. (2020); in this study, we consider the median of this range (period of 7.6 min = 456 s) for the wave period of the 2018 Anak Krakatau tsunami. We note that the tsunami source period of 6.3 – 8.9 min, reported by Heidarzadeh et al. (2020), is based on spectral analyses of coastal tide gauge records. Obviously, tsunami source periods remain the same along the journey from the source to the coast.

We apply our experimental data (Table 2) in combination with the field data of the 2018 Anak Krakatau event to produce our predictive equation. The nondimensional forms of the two parameters, slide volume (V/h^3) and landslide Froude number (F), are used. Based on the results of the previous section, we employ the same powers for these nondimensional parameters for our predictive equation. Our final equation for the nondimensional wave period ($T_M/\sqrt{\frac{h}{g}}$) is given in the following:

$$\frac{T_M}{\sqrt{h/g}} = 6.772\ (\frac{V}{h^3})^{0.678}/F^{\ 0.492} \quad (4)$$

where T_M is dominant wave period due to subaerial solid-block landslides in seconds, g is gravitational acceleration (9.81 m/s^2), F is Froude number (nondimensional), s is slide thickness in meters, V is slide volume in m^3, and h is water depth in meters. We note that Equation (4) is developed for a slope angle of 30^o.

We compare our predictive equation with three other equations proposed by Ataie-Ashtiani and Nik-Khah (2008), Heller and Spinneken (2013) and Heller and Spinneken (2015) in Table 3. For the case of the 2018 Anak

Krakatau event, the equations proposed by these authors result in wave periods of in the range of 390 s – 24,600 s, 40 s – 52 s, and 34 s – 35 s, respectively (Table 3). However, as the data of the 2018 Anak Krakatau tsunami was included in the database that we used for developing our predictive equation, it is natural that our equation gives a satisfactory prediction for the wave period of this tsunami in the range of 313 s – 670 s.

Figure 8 presents the performance of our predictive equation (Eq. 4) for estimating the experimental data of this study (Table 3) along with the 2018 Anak Krakatau event. Results indicate acceptable performances as the data points are aligned around the 45° line. To further validate the performance of our predicative equation, we tested it for one field landslide tsunami event (the Åkerneset event in Norway, Harbitz et al. 2014) whose data was not included in the database used for deriving the equation (Table 4). It can be seen that our predictive equation satisfactorily reproduces the wave period of this event.

Table 3. Comparison of the performance of our equation with that of three other existing equations for the prediction of the dominant period of the 2018 Anak Krakatau subaerial landslide tsunami. Parameters are: T_M, dominant wave period; V, landslide volume; h, water depth; and F, Froude number. The parameters of the 2018 Anak Krakatau event are based on the average values reported by Heidarzadeh et al. (2020), Grilli et al. (2019, 2021).

Author(s)	Predictive equation*	V (m³)	h (m)	s (m)	F	Observed T_M (s)**	Predicted T_M (s)
Ataie-Ashtiani and Nik-Khah (2008)	$\frac{T_M}{\sqrt{h/g}} = [4.14 + 3.88(V_1F^2)^2](\frac{T_{s1}}{V_1})^{-0.114} (\frac{l_s}{s})^{0.1} (\frac{r}{h})^{0.16}$	250 × 10⁶	100–200	100–250	1.0–1.40	378–534	390-24,600
Heller and Spinneken (2013)	$\frac{T_M}{\sqrt{h/g}} = \frac{19}{2}\left[F\left(\frac{s}{h}\right)^{0.5}\left(\frac{m_s}{\rho_w w h^2}\right)^{0.25}\left(\cos\frac{6}{7}\alpha\right)^{0.5} T_{s2}{}^{0.5}\right]^{1/4}$	250 × 10⁶	100–200	100–250	1.0–1.40	378–534	40-52
Heller and Spinneken (2015)	$\frac{T_M}{\sqrt{h/g}} = 5.5(\frac{m_s}{\rho_w w h^2})^{0.05} (\frac{r}{h})^{0.36}$	250 × 10⁶	100–200	100–250	1.0–1.40	378–534	34-35
This study	$\frac{T_M}{\sqrt{h/g}} = 6.772\ (\frac{V}{h^3})^{0.678}/F^{\ 0.492}$	250 × 10⁶	100–200	100–250	1.0–1.40	378–534	313-670

*: $T_{s1} = 0.43\ V_1^{-0.27} F^{-0.66}\ (\sin\alpha)^{1.32}$, the dimensionless slide underwater travel time, where V_1 is nondimensional slide volume defined as $V_1 = \frac{V}{wh^2}$, where w is slide width and V is slide volume; $T_{s2} = \frac{t_s}{[h+V/(s\ w)]/v_s}$, where t_s is characterise time of submerged landslide motion, $t_s = (\frac{h}{\tan\alpha})/v_s$ for cases with no transition; r (= 400 m) , distance from the impact point; w (=2000 m), slide width; s, slide thickness; l_s (=1000

m), slide length; m_s, slide mass (=6.25×10^{11}kg); ρ_w (=1000 kg/m^3), water density; α , slope angle; v_s(=44.9 m/s), slide velocity.

**: Based on Heidarzadeh et al. (2020).

Table 4. Application of our predictive equation to predict the subaerial landslide tsunami in Åkerneset, Norway as modelled by Harbitz et al. (2014). We note that this event is a hypothetical potential landslide tsunami. Parameters are: T_M, dominant wave period; V, landslide volume; h, water depth; v_s, landslide velocity; and F, Froude number.

Event name	Predictive equation	V (m^3)	h (m)	v_s (m/s)	F	Reported T_M (s)**	Predicted T_M (s)
Åkerneset	This study	54×10^6	250 – 300	70 – 80	1.3 – 1.6	~ 60	49 – 66

**: Based on Harbitz et al. (2014).

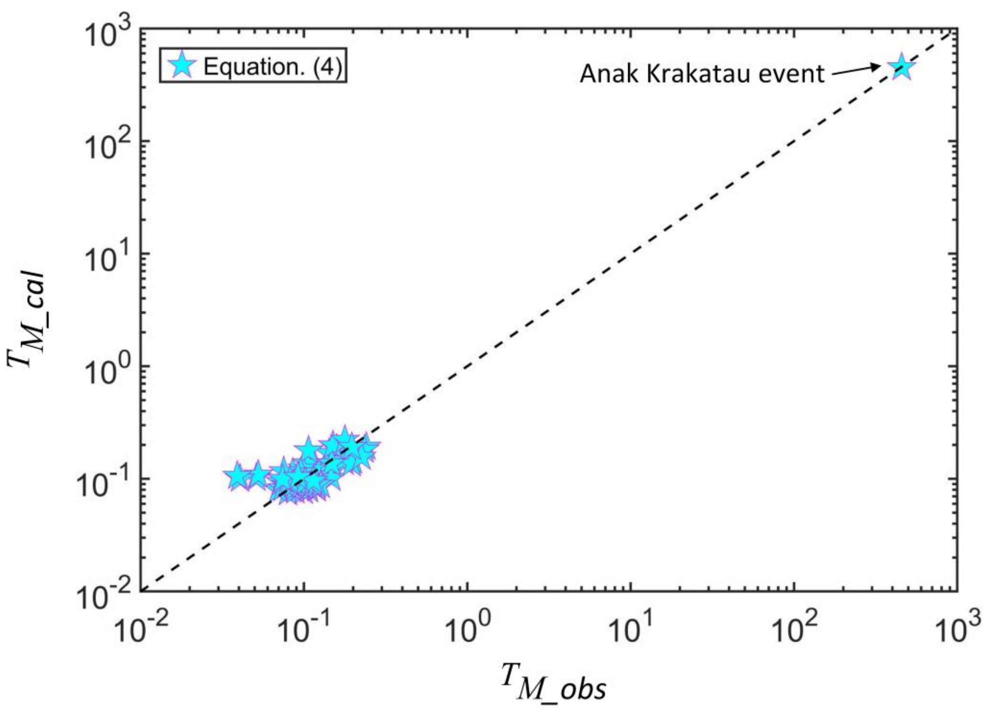

Figure 8. Performance of the developed predicative equation in this study (T_{M_cal}, Eq. 4) in reproducing experimental data (T_{M_obs}).

5-Conclusions

We conducted a physical modelling study, involving 51 laboratory experiments, to investigate the period of the wavs generated by subaerial solid-block landslide tsunamis. The laboratory data combined with field data (i.e., the 2018 Anak Krakatau event) were employed to develop a new predictive equation. The findings are:

- Our experimental data revealed that a direct relationship exists between the dominant wave period and landslide volume.
- Regarding the Froude number of the landslides, our experiments resulted in an inverse relationship between the Froude number and wave period.
- A combination of laboratory data and field data from the 2018 Anak Krakatau event were employed to develop a new predictive equation for the wave period of subaerial solid-block landslide tsunamis. This equation is made of three landslide parameters namely landslide volume, water depth and landslide Froude number.
- The performance of the new predictive equation was compared with that of previously-published equations and was tested against an independent field event, whose data was not included for the derivation of our equation. It was shown that our equation performs satisfactorily.

Acknowledgements

We are grateful to laboratory technicians, in particular Charles Morrison, who supported us during the physical experiments.

Funding

This research is funded by the Royal Society (the United Kingdom) grant number CHL/R1/180173. We also acknowledge funding from the Lloyd's Tercentenary Research Foundation, the Lighthill Risk Network, and the Lloyd's Register Foundation-Data Centric Engineering Programme of the Alan Turing Institute.

Data availability statement

All data used in this study are given in the body of the article.

Declaration of interest

The authors declare that they have no competing interests regarding the work presented in this paper.

Reference

Aránguiz, R., Esteban, M., Takagi, H., Mikami, T., Takabatake, T., Gómez, M., et al. 2020. "The 2018 Sulawesi tsunami in Palu city as a result of several landslides and coseismic tsunamis." *Coastal Engineering Journal* 62 (4): 445-459.

Ataie-Ashtiani, B., and A. Nik-Khah. 2008. "Impulsive waves caused by subaerial landslides." *Environmental Fluid Mechanics* 8 (3): 263-280.

Bullard, G. K., R. P. Mulligan, A. Carreira, and W. A. Take. 2019. "Experimental analysis of tsunamis generated by the impact of landslides with high mobility." *Coastal Engineering* 152: 103538.

Fritz, H. M., W. H. Hager, and H.-E. Minor. 2004. "Near field characteristics of landslide generated impulse waves." *Journal of Waterway, Port, Coastal, and Ocean Engineering* 130 (6): 287-302.

Grilli, S. T, C. Zhang, J. T. Kirby, A. R., Grilli. D. R., Tappin. S. F. L., Watt. et al. 2021. "Modeling of the Dec. 22nd 2018 Anak Krakatau volcano lateral collapse and tsunami based on recent field surveys: Comparison with observed tsunami impact." *Marine Geology* 440: 106566.

Grilli, S. T., D. R. Tappin., S. Carey, S. F. Watt, S. N. Ward, A. R. Grilli, et al. 2019. "Modelling of the tsunami from the December 22, 2018 lateral collapse of Anak Krakatau volcano in the Sunda Straits, Indonesia." *Scientific reports* 9 (1): 1-13.

Heidarzadeh, M., T. Ishibe, O. Sandanbata, A. Muhari, and A. B. Wijanarto. 2020. "Numerical modeling of the subaerial landslide source of the 22 December 2018 Anak Krakatoa volcanic tsunami, Indonesia." *Ocean Engineering* 195: 106733.

Heidarzadeh, M., K. Satake. 2015. "Source properties of the 1998 July 17 Papua New Guinea tsunami based on tide gauge records. " *Geophysical Journal International* 202(1):361-369.

Heller. V. 2011. "Scale effects in physical hydraulic engineering models." *Journal of Hydraulic Research* 49 (3): 293-306.

Heller. V, and J. Spinneken. 2013. "Improved landslide-tsunami prediction: effects of block model parameters and slide model." *Journal of Geophysical Research* 118 (3): 1489-1507.

Heller, V, and W. H. Hager. 2011. "Wave types of landslide generated impulse waves". *Ocean Engineering* 38 (4): 630-640.

Heller, V, and J. Spinneken. 2015. "On the effect of the water body geometry on landslide–tsunamis: Physical insight from laboratory tests and 2D to 3D wave parameter transformation." *Coastal Engineering* 104: 113-134.

Hughes, S. A. 1993. "Physical models and laboratory techniques in coastal engineering." World Scientific. 588 pages.

Lighthill, J. (1978). "Waves in fluids." Cambridge, Cambridge University Press, 1978. 516 p.

McFall, B. C, and H. M. Fritz. 2016. "Physical modelling of tsunamis generated by three-dimensional deformable granular landslides on planar and conical island slopes." *Proceedings of the Royal Society A* 472 (2188): 20160052.

Mohammed, F., and H. M. Fritz. 2012. "Physical modelling of tsunamis generated by three-dimensional deformable granular landslides." *Journal of Geophysical Research: Oceans* 117 (C11).

Muhari, A., M. Heidarzadeh, H. Susmoro, H. D. Nugroho, E. Kriswati, A. B. Wijanarto. 2019. "The December 2018 Anak Krakatau Volcano tsunami as inferred from post-tsunami field surveys and spectral analysis." *Pure and Applied Geophysics* 176.12: 5219-5233

Mulligan, R. P., and W. A. Take. 2017. "On the transfer of momentum from a granular landslide to a water wave." *Coastal Engineering* 125: 16-22.

Mulia, I. E., S. Watada, T. C. Ho, K. Satake, Y. Wang, and A. Aditiya. 2020. "Simulation of the 2018 tsunami due to the flank failure of Anak Krakatau volcano and implication for future observing systems." *Geophysical Research Letters* 47 (14): e2020GL087334.

Noda, E. 1970. "Water waves generated by landslides." *Journal of the Waterways, Harbors and Coastal Engineering Division* 96 (4): 835-855.

Paris, A., P. Heinrich, R. Paris, and S. Abadie. 2020. "The December 22, 2018 Anak Krakatau, Indonesia, landslide and tsunami: preliminary modeling results." *Pure and Applied Geophysics*, 177 (2): 571-590.

Panizzo A, P.D. Girolamo, M.D. Risio, A. Maistri, A. Petaccia. 2005. "Great landslide events in Italian artificial reservoirs." *Natural Hazards and Earth System Sciences* 5: 733–740.

Ren, Z., Y. Wang, P. Wang, J. Hou, Y. Gao, and L. Zhao. 2020. "Numerical study of the triggering mechanism of the 2018 Anak Krakatau tsunami: eruption or collapsed landslide?" *Natural Hazards* 102 (1): 1-13.

Sælevik, G., A. Jensen, and G. Pedersen. 2009. "Experimental investigation of impact generated tsunami; related to a potential rockslide, Western Norway." *Coastal Engineering* 56 (9): 897-906.

Synolakis, C.E., Bardet, J.P., Borrero, J.C., Davies, H.L., Okal, E.A., Silver, E.A., Sweet, S. and Tappin, D.R., 2002. "The slump origin of the 1998 Papua New Guinea tsunami." Proceedings of the Royal Society of London. *Series A: Mathematical, Physical and Engineering Sciences* 458 (2020): 763-789.

Takabatake, T., Mäll, M., Han, D. C., Inagaki, N., Kisizaki, D., Esteban, M., and Shibayama, T. 2020. "Physical modeling of tsunamis generated by subaerial, partially submerged, and submarine landslides." *Coastal Engineering Journal* 62 (4): 582-601.

Takagi, H., M. B. Pratama, S. Kurobe, M. Esteban, R. Aránguiz, and B. Ke. 2019. "Analysis of generation and arrival time of landslide tsunami to Palu City due to the 2018 Sulawesi earthquake." *Landslides* 16 (5): 983-991.

Van Nieuwkoop, J.C.C. 2007. "Experimental and numerical modelling of tsunami waves generated by landslides." MSc thesis at the faculty of civil engineering and geosciences at Delft University of Technology, The Netherlands.

Zengaffinen, T., F. Løvholt, G. K. Pedersen, and A. Muhari. 2020. "Modelling 2018 Anak Krakatoa Flank Collapse and Tsunami: effect of landslide failure mechanism and dynamics on tsunami generation." *Pure and Applied Geophysics* 177 (6): 2493-2516.

Table captions:

Table 1. Geometrical information of the four solid blocks used for landslide physical experiments in this study.

Table 2. The experimental program for the 51 physical tests performed in this study for subaerial solid-block landslide-generated waves. All experiments are conducted using a slope angle of 30°. Parameters are: F, Froude number; h, water depth; D, travel distance (the distance from toe of the sliding mass to the water surface); T_M, dominant wave period; a_M, maximum wave amplitude; M_s, nondimensional mass; L_M, dominant wavelength; and U, Ursell number. See Figure 1 for the sketch showing some of these parameters.

Table 3. Comparison of the performance of our equation with that of three other existing equations for the prediction of the dominant period of the 2018 Anak Krakatau subaerial landslide tsunami. Parameters are: T_M, dominant wave period; V, landslide volume; h, water depth; and F, Froude number. The parameters of the 2018 Anak Krakatau event are based on the average values reported by Heidarzadeh et al. (2020), Grilli et al. (2019, 2021).

Table 4. Application of our predictive equation to predict the subaerial landslide tsunami in Åkerneset, Norway as modelled by Harbitz et al. (2014). We note that this event is a hypothetical potential landslide tsunami. Parameters are: T_M, dominant wave period; V, landslide volume; h, water depth; v_s, landslide velocity; and F, Froude number.

Figures captions:

Figure 1. Sketch showing the geometrical and kinematic parameters of a subaerial landslide tsunami. Parameters are: h, water depth; a_M, maximum wave amplitude; α, slope angle; L_M, dominant wavelength; l_s, length of slide; D, travel distance (the distance from toe of the sliding mass to the water surface); and SWL, still water level.

Figure 2. Wave flume used in this study for physical experiments showing the wave gauge (WG), the slope **(a),** and the four sliding blocks **(b)**. Parameters are: h, water depth; D, travel distance (the distance from toe of the sliding mass to the water surface); SB_{1-4}, Solid blocks (see Table 1 for their dimensions). The distance between the toe of slope and the wave gauge is 0.40 m.

Figure 3. Studying the effect of landslide volume on the experimental water waveforms recorded for the solid-block subaerial landslide-generated waves during the physical modelling using different concrete blocks with volumes V_1 - V_4 (Table 1) at different water depths (h) and Froude numbers (F). The horizontal axis shows time (t), and the vertical axis shows wave amplitude (η).

Figure 4. Studying the effect of Froude number on the experimental water waveforms recorded for solid-block subaerial landslide-generated waves during the physical modelling using different concrete blocks with volumes V_1 - V_4 (Table 1), different water depths (h) and Froude numbers (F). The horizontal axis shows time (t), and the vertical axis shows wave amplitude (η).

Figure 5. A 3D projection of the maximum wave amplitudes (a_M) of our experimental data versus solid block volumes (V) and water depths (h).

Figure 6. Nondimensional waveforms for pairs of physical experiments with similar nondimensional mass (M_s) and Froude number (F) as a way to study scale effects during our physical modelling. V_1, V_2 and V_3 are different concrete blocks (Table 1), h is water depth, η is wave amplitude, t is time, and g is gravitational acceleration.

Figure 7. Curve fitting on the experimental data of dominant wave period (T_M). (**a**) The effect of volume of sliding mass (V) on the wave period. F_{Ave} is the average Froude number for each group of the tests. For this analysis, tests with the same release mechanism (i.e., gravity; F≅0.36) and the same water depth but with different slide volumes were grouped together. (**b**) The effect of Fronde number of the landslides (F) on the wave period. Here, h is water depth, and g is gravitational acceleration. For this analysis, tests with the

same water depths and the same volumes but different Froude number were grouped together. SD is abbreviation for standard deviation.

Figure 8. Performance of the developed predicative equation in this study (T_{M_cal}, Eq. 4) in reproducing experimental data (T_{M_obs}).